



Review

Semiconductor/boron nitride composites: Synthesis, properties, and photocatalysis applications



Chengyun Zhou¹, Cui Lai¹, Chen Zhang¹, Guangming Zeng*, Danlian Huang*, Min Cheng, Liang Hu, Weiping Xiong, Ming Chen, Jiajia Wang, Yang Yang, Longbo Jiang

College of Environmental Science and Engineering, Hunan University and Key Laboratory of Environmental Biology and Pollution Control (Hunan University), Ministry of Education, Changsha, 410082, PR China

ARTICLE INFO

ABSTRACT

Keywords:

Boron nitride
Semiconductor photocatalysis
Immigration of electrons and holes
Pollutant degradation

Semiconductor photocatalysis has been regarded as one of promising approach to solve the environmental pollution and energy crisis. Boron nitride (BN), as a new nanomaterial, has distinct structures and properties that can add attractive properties to photocatalysts. In the past few years, many encouraging achievements have been made in the research field of BN-based semiconductor photocatalysts. Semiconductor/BN composites have attracted extensive attention due to its well photocatalytic activity. This work summarized recent progress on the synthesis of BN and semiconductor/BN composites. These semiconductor/BN composites have various applications in photocatalytic fields, such as pollutant degradation and photocatalytic hydrogen evolution. The role of BN in semiconductor/BN composites is discussed in depth. Coupling BN with semiconductors can improve the photocatalytic activity of semiconductors due to their surface charge transfer properties. The photocatalytic mechanisms and different types of photocatalysts are studied. Furthermore, perspectives on semiconductor/BN composites are discussed, including the challenges for large scale preparations and theoretical calculation of composites. It is expected that this review would be helpful for designing of highly efficient semiconductor/BN composites.

1. Introduction

Sustainable supply of green energy and environmental pollution are two of the main global challenges of the current era. Clean and safe water is an essential resource for the life and health for human [1–6]. However, around 1.2 billion people still have insufficient amounts of this resource around the world [7,8]. With the fast industrialization development, more and more wastewaters containing organic pollutants and heavy metals was produced, which caused serious threats to the environment and drinking water [9–14]. These contaminants are resistant to conventional water and wastewater treatment, which may pose risks to human and ecological systems even at trace level [15–20]. Advanced Oxidation Processes (AOPs) was regarded as an effective technique for the degradation of organic contaminants, owing to the creation of highly reactive radicals (e.g. $\cdot\text{OH}$, $\cdot\text{O}_2^-$, and $\cdot\text{SO}_4^{2-}$) [21–24]. Lately, visible light response photocatalysts arouse enormous attention for applications in environmental and energy areas.

Semiconductor based photocatalysis is one of the most promising technologies to solve the energy and environmental crisis [25–27]. A

number of photocatalysts were synthesized and used for light induced chemical transformations, such as ZnO [28], TiO_2 [29,30], CdS [31], and $\text{g-C}_3\text{N}_4$ [32–36]. When the photon energy of light is higher than the band gap of photocatalyst, electrons can be excited and transferred from the valence band (VB) to the conduction band (CB), leading to electron-hole separation. These charge carriers will migrate to the surface to initiate the chemical reaction [37,38]. Photogenerated holes and electrons could be utilized for contaminants degradation, water splitting, and disinfection. However, the charge carriers can easily recombine. The emerging nanomaterials as the new building blocks to construct light energy harvesting assemblies has opened up new ways to utilize renewable energy resources due to their large surface areas, abundant surface states, and diverse morphologies.

Among them, hexagonal boron nitride (h-BN), a two-dimensional (2D) network of hexagonal structured material, has attracted a lot of research interest [39,40]. The h-BN is composed of equal numbers of boron (B) and nitrogen (N) atom, and it was thought to be a type of synthetic material [41,42]. The h-BN is called “white graphene” or “non-carbon graphene” due to the analogue 2D atomic crystal structure

* Corresponding authors at: College of Environmental Science and Engineering, Hunan University, Changsha, Hunan, 410082, China.

E-mail addresses: zgming@hnu.edu.cn (G. Zeng), huangdanlian@hnu.edu.cn (D. Huang).

¹ These authors contribute equally to this article.

and van der Waals heterojunction [43,44]. The h-BN possesses a high thermal conductivity ($600 \text{ W m}^{-1} \text{ K}^{-1}$), a wide band gap (5.2–5.5 eV) and a high surface area ($3300 \text{ m}^2 \text{ g}^{-1}$) [45]. These unique properties indicate that h-BN has great potential to be applied in adsorption [46–48], energy storage [49–51], and catalysis [52–54]. With the rapid development of h-BN preparation technology, the h-BN based nanomaterials for applications in photocatalytic field are also under fast development. Many important findings have been reported on the h-BN based nanomaterials during the past few years, such as $\text{TiO}_2/\text{h-BN}$ [55,56], $\text{g-C}_3\text{N}_4/\text{h-BN}$ [57]. BN-based photocatalysts present higher photocatalytic activity than its single photocatalyst due to their surface properties. The photocatalytic enhancement is generally ascribed to the suppressed recombination of photogenerated electron–hole pairs, extended excitation wavelength and increased surface-adsorbed reactant. As the field of semiconductors/h-BN composite advancing, a comprehensive review regarding on the latest developments is necessary and urgent at this stage.

In this review, we briefly introduce the fabrication of the BN and BN-based materials, followed by placing emphases on recent development about the applications of BN-based materials as catalysts in the environmental remediation and energy conversion. Finally, the challenge and perspectives for future development are discussed. We hope that this paper would be helpful for designing and fabricating novel semiconductor/BN photocatalysts with greater performances in the near future.

2. Syntheses of BN and semiconductor/BN composites

2.1. Syntheses of BN

Boron is a lightweight and metalloid element that is generally capable of forming stable covalent bonds in crystalline structures with boron in the oxidation state III. BN is the most promising and popular inorganic nonmaterial [58,59]. Recently, BNs have been discovered in natural mineral and in several different forms, including graphite-like hexagonal boron nitride (g-BN or h-BN), cubic boron nitride (c-BN), wurtzite boron nitride (w-BN), and amorphous boron nitride (a-BN). Among these forms, the h-BN is the representative crystal structures of BNs [60]. To date, many methods have been applied in the preparation of BN, which have similarities to the methods used to fabricate graphene, including ball milling, template approach, and template-free approach. Different synthetic methods for BN materials have been summarized in Table 1. To achieve better dispersion and enlarge the application of BN, methods like chemical modification have been employed.

2.1.1. Mechanical exfoliation technique

Mechanical exfoliation technique was often used to separate the multilayer graphene [61]. Layered h-BN nanosheet can also be prepared by this technique. Urea was employed to assist exfoliation of the h-BN by ball milling method. This ambient temperature method has several advantages, including scalability for mass production, low cost, high yield without organic solvents. Similarly, Lee et al. prepared hydroxyl-functionalized BN nanoplates (OH-BNNPs) by a simple ball milling of BN powders in the presence of sodium hydroxide (Fig. 1a) [62]. Fig. 1b shows low-magnification TEM images indicating that there are thin 2D nanoplates in solution. The inset figure shows selected area electron diffraction (SAED) pattern measured along the (0001) zone axis, which exhibits typical 6-fold symmetry of h-BN, suggesting that the hexagonal lattices of the OH-BNNPs were not damaged during the exfoliation processes.

2.1.2. Template approach

The template approach is the most widely reported and successfully used method for the introduction of mesoporous in solid materials such as carbon, polymers and ceramics [63,64]. For example, Bios et al. primarily prepared a ordered mesoporous boron nitride (MBN) by using CMK-3 mesoporous carbon as a template and tri(methyl-amino)borazine as a boron nitride source [65]. The specific surface area ($540 \text{ m}^2 \text{ g}^{-1}$), and the mesoporous volume ($0.27 \text{ cm}^3 \text{ g}^{-1}$) of BN are higher than that of the non-porous BN. Vinu et al. reported the preparation of mesoporous boron nitride (MBN) with a very high surface area and pore volume [66]. The materials were fabricated via substitution reactions at high temperatures ($1500\text{--}1750^\circ\text{C}$), using a well-ordered hexagonal mesoporous carbon as a template and boron trioxide as a boron source. The specific surface area and the specific pore volume of MBN are $565 \text{ m}^2 \text{ g}^{-1}$, and $0.53 \text{ cm}^3 \text{ g}^{-1}$, respectively. Schlienger et al. prepared MBN-based materials template of zeolites [67]. The overall synthetic path of zeolite-derived BN-based materials was presented in Fig. 2. Maleki et al. developed a facile procedure for the synthesis of BN with hierarchical porous structure using CTAB and PS as dual inorganic templates [68].

Soft template approach is also an interesting strategy, which has been applied for the synthesis of various porous BN materials. Block polymers such as P123 and P127 have been used in the preparation of BN materials. Li et al. demonstrated that the mixture of P123 and BN precursors (Boric acid and melamine) could obtain the porous ribbon-like microstructure BN [69]. The BET surface area of BN was found to be $2700 \text{ m}^2 \text{ g}^{-1}$, and the pore volume was up to $1.66 \text{ cm}^3 \text{ g}^{-1}$. The addition of P123 in this work not only increases the surface area and pore volume but also enhances the adsorption ability of the pristine BN. The porous BN can be as a promising material applied for environmental remediation.

Table 1
Summarization of different synthetic methods for BN materials.

Name	Synthetic Method	Template/Precursors	Morphology	Pore volume ($\text{cm}^3 \text{ g}^{-1}$)	Specific surface area ($\text{m}^2 \text{ g}^{-1}$)	ref
activated BN BN-1200	Hard template	Activated carbon/ B_2O_3	Ribbon structure	0.27	168	[63]
	Hard template	Zeolite/polyborazylene	Porous architecture	0.8	570	[67]
BN	Hard template	CMK-3/ trimethylaminoborazine	Porous texture	0.25	540	[64]
HPBN	Hard template	Polystyrene (PS) and CTAB/ammonia borane	Hierarchical porous structure	0.68	443	[68]
MBN	Hard template	Mesoporous carbon/ B_2O_3	Rod-like morphology	0.53	565	[66]
BN	Soft template	P123/Boric acid and melamine	Porous, rippled, and corrugated ribbons	1.66	2078	[69]
BN	Template-free	Ammonium fluoroborate	hollow nanospheres	1.41	318.7	[75]
BN	Template-free	Boric acid and urea	Thin layer	–	927	[72]
BN-200	Template-free	Boric acid and urea	flake-like morphology	0.869	1016	[73]
BN	Template-free	Boron trioxide and guanidine hydrochloride	Porous nanosheets	1.09	1427	[60]
3D BN	Template-free	Boron trioxide and urea	Curly and interconnected sheets	1.17	1156	[47]
h-BNNs	Template-free	Boric acid and urea	Curly and flat layers	–	1900	[70]
h-BN	Template-free	Boric acid and melamine	stacked layer	0.49	964.4	[71]

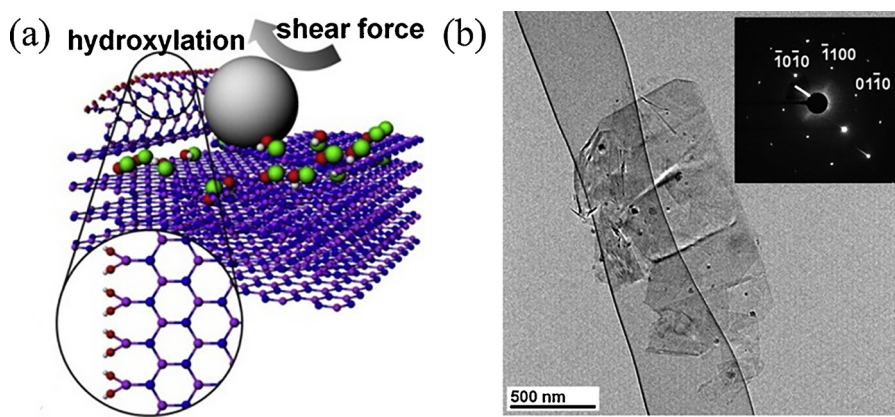


Fig. 1. (a) Thin curled sheets peeling off the top surface of an h-BN particle in response to shear forces created by the milling balls. (b) Low-magnification TEM image of OH-BNNPs and corresponding selected-area diffraction (SAED) patterns. Reproduced with permission from Ref. [62]. Copyright 2015, ACS.

2.1.3. Template-free approach

Hard or soft templates have many disadvantages, such as tedious synthesis procedures, difficult in removing the template completely, long preparation time and high cost, which limit their extensive applications in a large-scale. Recently, a variety of porous BN with different structure and morphology have been synthesized by the self-assembly and template-free methods [70,71]. Nag and co-workers demonstrated that the thin graphene analogue BN layers could be obtained via the polymerization of boric acid and urea at 900 °C in N₂ atmosphere [72]. The surface area of the BN can be controlled by the layer thickness. When the ratio of boric acid to urea is 1–48, the sample could achieve the thinnest BN layer with a surface area of 927 m² g⁻¹ and a high CO₂ uptake. This simple method has enabled us to prepare graphene analogue BN with varying thicknesses. The details of the reaction are explained by the following equations (Eq. (1)–(3)).



Interestingly, Wu et al. recently synthesized h-BNs with varying surface areas relying on the solvents used during the preparation steps of the precursors [70]. Solvents and drying time had an effect on the crystalline structure of the intermediates [73]. For example, Marchesini and co-workers have developed a template-free method to produce BN with tunable surface area and micro/mesoporosity by using multiple N-containing precursors in Fig. 3 [74]. The optimized sample exhibit a surface area of 1400 m² g⁻¹ and enhanced CO₂ capture capacity compared to commercial zeolites. In addition, the BN can be shaped as pellets with little or no reduction in porosity and gas uptake.

In addition, Lei et al. synthesized highly porous BN nanosheets by the simple thermal condensation of boron trioxide and guanidine hydrochloride [60]. The mixture was heated in a flowing nitrogen-15% hydrogen atmosphere at 1100 °C for 2 h. The resulting product could

exhibit a high surface area of 1427 m² g⁻¹ and a pore size distribution ranging from 20 to 100 nm. The material shows excellent sorption performances for a wide range of oils, solvents and dyes, with mass uptakes reaching 3300%, which was due to a combination of super hydrophobicity, porosity and swelling ability.

2.2. Syntheses of semiconductor/BN composites

A variety of semiconductors have been employed to the synthesis of semiconductor/BN composites, such as metal oxides and metal sulfides (e.g. TiO₂, ZnO, WO₃ and CdS), bismuth based semiconductor (e.g. BiOBr, BiOCl, Bi₄O₅Br₂, and BiOI), and silver based semiconductor (e.g. AgI, AgBr, Ag₃PO₄, AgVO₄, and AgCrO₄) and metal-free semiconductor (e.g. graphitic carbon nitride). The widely preparation methods are including *in-situ* growth, precipitation, ball milling, hydrothermal and/or solvothermal method, which are summarized in Table 1. Here, the following passages will give a more detailed description of the available synthesis routes.

2.2.1. *In-situ* growth method

The *in-situ* growth method is widely used to prepare the BN based composites. The precursor of metal salt could be transformed into metal oxides and then deposited on the surface of BN, and then forming the BN based composite. Tang et al. constructed BN/TiO₂ composite through the hydrolysis of TiCl₃ in the ethanol-water aqueous solution with BNNTs [75]. This method involves the reaction of Ti³⁺ with the oxidized radicals BN-H⁺ to form BN-Ti⁴⁺ bonds firstly, and *in-situ* hydrolytic conversion of the attached Ti⁴⁺ into TiO₂. Ide et al. also used TiCl₃ as precursor and *in-situ* growth TiO₂ with BN [76]. Then, the Au/TiO₂/BN could be obtained through the HAuCl₄ 3H₂O and the as-prepared TiO₂/BN. Tetrabutyl titanate (Ti(OC₄H₉)₄) is another precursor of TiO₂. For example, BN/TiO₂ composites were fabricated via water-phase synthesis by Liu et al., who used porous BNNSs and Ti(OC₄H₉)₄ as the starting materials [77]. After stirring and heating, the TiO₂

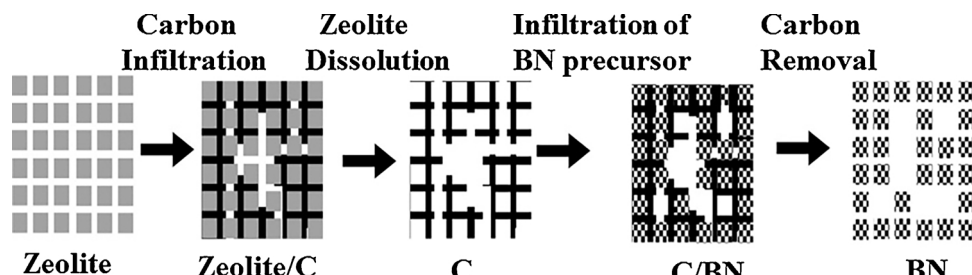


Fig. 2. Overall synthetic path employed to generate zeolite-derived BN-based materials with micro- and mesoporosity. Note that the last structure is in fact disorganized. Reproduced with permission from Ref. [67]. Copyright 2011, ACS.

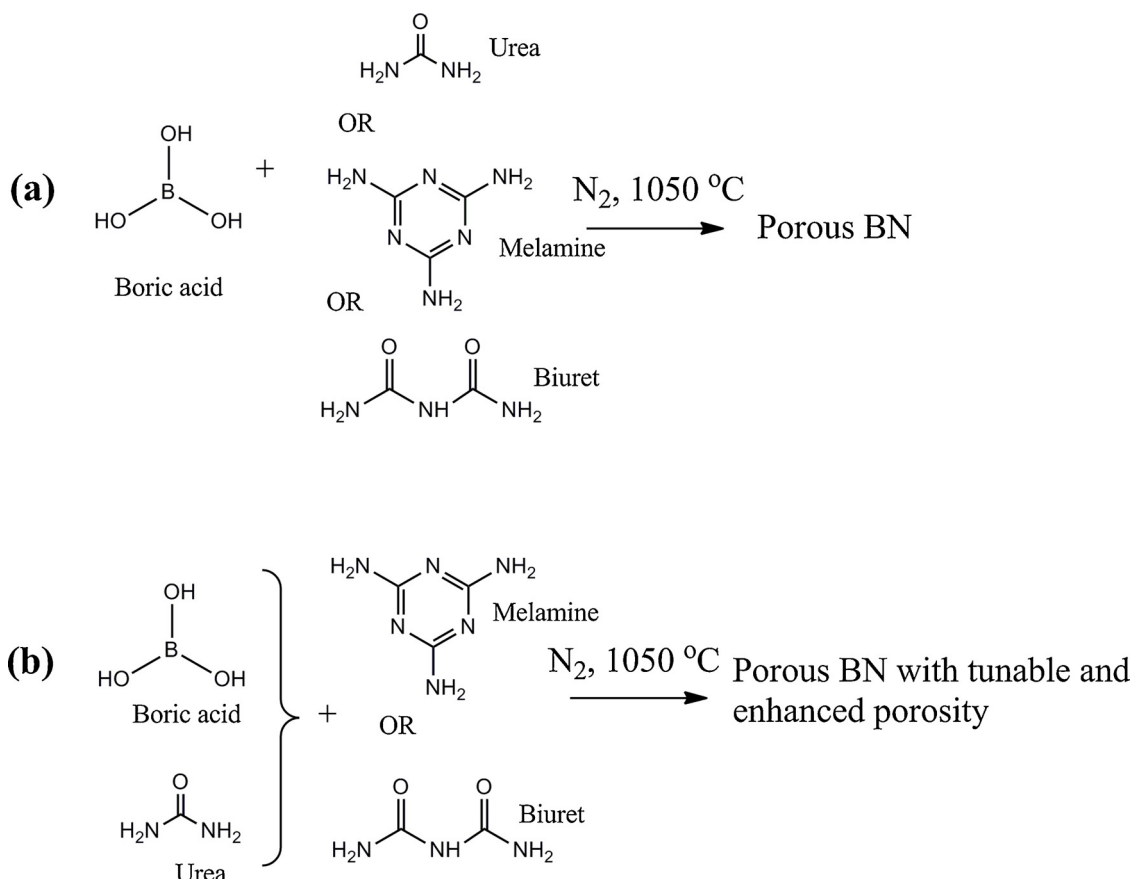


Fig. 3. Template-free synthesis methods for porous boron nitride using (a) a single N-containing precursor route; (b) a two N-containing precursors route.

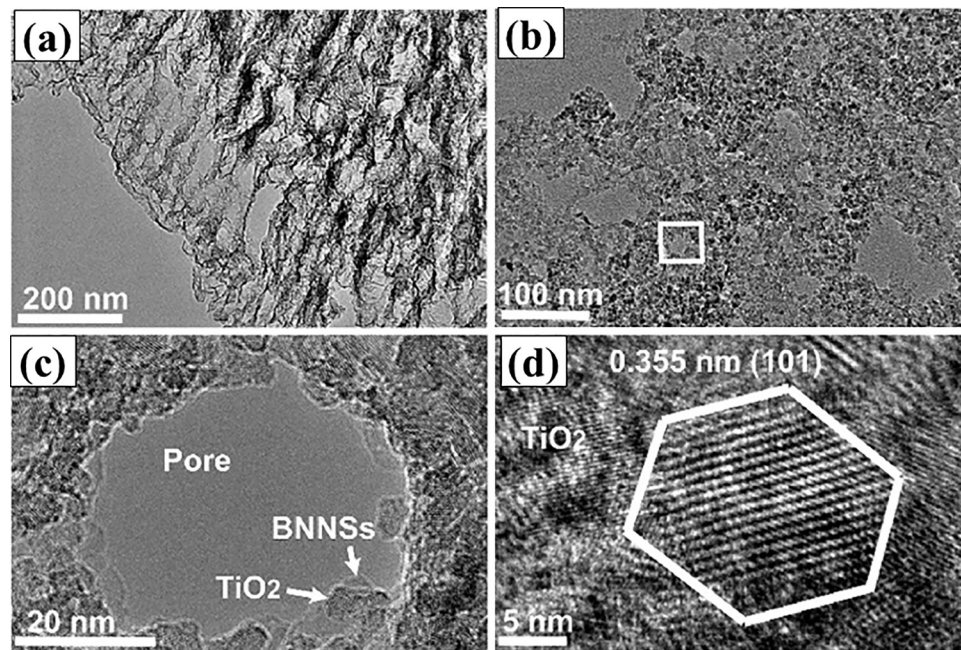


Fig. 4. TEM images of (a) porous BNNSs and (b) porous BN/TiO₂ hybrid nanosheets (TiO₂: 38 wt%). (c) and (d) HRTEM images for a hole decorated by TiO₂ nanoparticles from the rectangular area in (b), and a single TiO₂ particle as indicated by the white arrow in (c). Reproduced with permission from Ref. [77]. Copyright 2017, elsevier.

nano-particles were deposited on the surface of the BN as it is hydrolyzed. As shown in Fig. 4, The TEM image of porous BNNSs/TiO₂ (38 wt %) hybrid nanosheets shows that the TiO₂ nanoparticles were loaded homogeneously on porous BNNSs. The HRTEM image of TiO₂ nanoparticles indicated a well-defined crystallinity of TiO₂ with lattice spacing of 0.355 nm, which corresponded to the (101) planes of anatase

phase. In addition, Wang and co-workers developed a facile *in-situ* growth method with the hydrolysis of SnCl₂ in the presence of BN acid aqueous solution to obtain the BN/SnO₂ composite [78]. The *in situ* growth strategy can avoid the agglomeration of the semiconductor nanoparticles on the BN.

A variety of silver-based semiconductor photocatalysts can also be

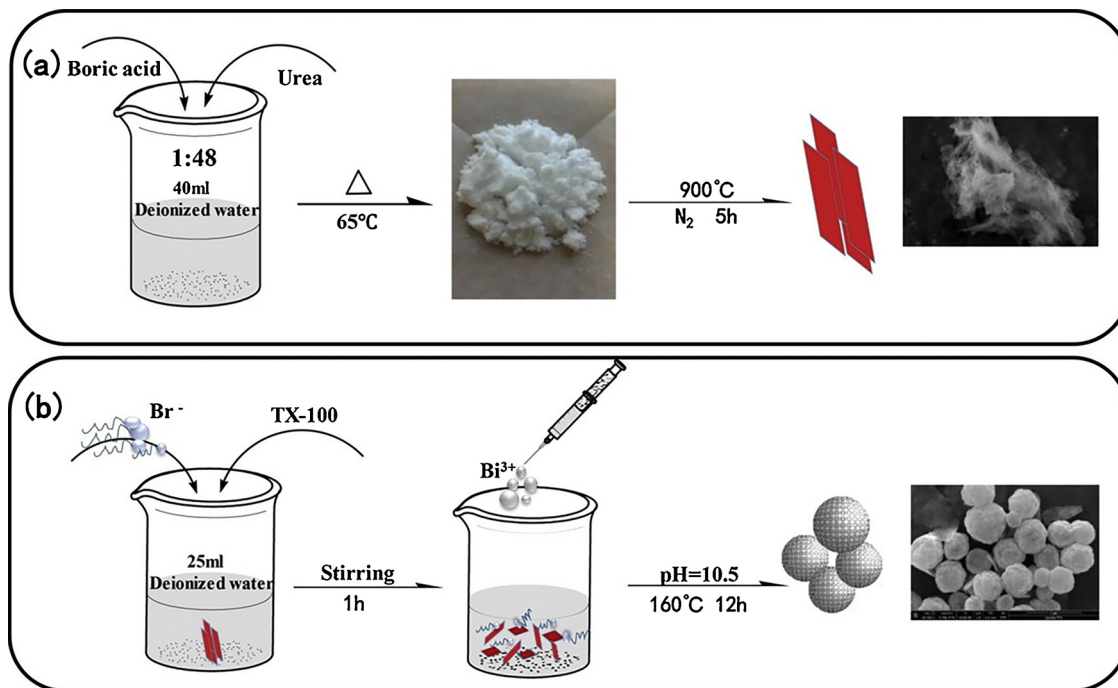


Fig. 5. Schematic illustration of the synthetic process for (a) graphene-analogue h-BN and (b) h-BN/Bi₄O₅Br₂ composites. Reproduced with permission from Ref. [97]. Copyright 2017, Elsevier.

immobilized on to BN materials by *in-situ* growth strategy. For example, Choi et al. prepared a two-component composite of AgI/BN by an *in-situ* ultrasound assisted method. They added an aqueous solution of BN and AgNO₃ dropwise into a KI solution [79]. AgI was formed at the surface of BN sheets at room temperature. In order to get enhanced photocatalytic activity of AgI/BN photocatalyst, Wu and co-workers synthesized a navy bean shaped AgI/AgBr biphasic heterostructures loaded on few-layered h-BN nanosheets [80]. The BN and AgBr were first dispersed in deionized water and sonicated. Then KI aqueous solution was added into the mixture solution and stirred for anion exchange. Polyvinyl pyrrolidone (PVP), as an excellent dispersant, was to protect the silver nanoparticles from growing and agglomerating [81]. Zhu et al. deposited Ag₃PO₄ nanoparticles on the h-BN nanosheets via the simple precipitation method [82]. Amount of h-BN and PVP were suspended in aqueous solution, and then the AgNO₃ aqueous solution and Na₂HPO₄ aqueous solution were added into the above h-BN solution under dark condition. Apart from this material, other silver based BN composites have been prepared via this method, such as BN/AgBr [83], BN/AgCrO₄ [84], BN/Ag₂CO₃ [85], and BN/Ag₃VO₄ [86].

Graphene carbon nitride (g-C₃N₄), a non-metal material, is regarded as a promising visible light driven photocatalyst. The catalytic performance of g-C₃N₄ can be improved by the hybridization with other 2D materials, such as graphene and its derivatives. Recently, our group prepared the g-C₃N₄/BN composites by a facile *in-situ* growth strategy [87]. We used h-BN and dicyandiamide as precursor, calcined at 550 °C, and then g-C₃N₄/BN was obtained. g-C₃N₄ was deposited on the surface of BN sheets due to the π - π interaction of structure between g-C₃N₄ and BN. Very recently, He and co-worker reported the direct growth of g-C₃N₄ on the h-BN porous nanosheets [88]. The g-C₃N₄/h-BN composite was obtained by using the boric acid and urea as the source of h-BN, and using urea as precursors of g-C₃N₄.

2.2.2. Ball milling method

Ball-milling is a very effective method to prepare the solid-solid composites, which can enhance the reactivity of the reagents due to mechanical breaking of molecular bonds. Ball-milling has been used to prepared photocatalyst composites. Since the BN is formed by the

rolling up of sheet, more accessible layer structure may achieve better electrostatic distribution. Chen et al. used water as solvent and different contents of BN to prepared h-BN/TiO₂ via ball milling [89]. Through milling process, the h-BN and TiO₂ can be connected closely, and then the charged h-BN could promote the immigration of holes from the bulk of TiO₂ to its surface. Similarly, Fu et al. also fabricated the h-BN/ZnO by these above methods [90]. For further restrain the recombination of photogenerated electron–hole pairs of CdS, it is also possible to use the exfoliated h-BN as the holes capturer. Zhang et al. synthesized the BN/CdS composite samples by ball milling method [91]. The bulk h-BN was milled into some flake and was combined with CdS in the ball-milling process.

2.2.3. Solvothermal/hydrothermal method

The solvothermal method is an effective approach to the preparation of semiconductors/BN composites. Recently, Xie et al. found a route for the preparation of TiO₂/BN with the hydrothermal method using the ethanol as solvent [92]. Considering the poor dispersion of h-BN in water, ionic liquid was added to improve the dispersion. The BN/BiPO₄ composite was obtained when Bi(NO₃)₃·5H₂O and ionic liquid (Omim H₂PO₄) was mixed with BN nanosheet in ethanol and heated at 160 °C for 24 h in oven [93]. Similarity, A graphene-like BN modified BiOBr materials were also fabricated by 1-hexadecyl-3-methylimidazolium bromide (C₁₆mim Br) ionic liquid assisted solvothermal method [94]. In addition, the BN based composites with distinct morphology has also been prepared by this method [95]. For example, Liu et al. fabricated 3D hierarchical microsphere BN/BiOI composite by a solvothermal method [96]. Other Bi-based semiconductors have also been integrated with BN by this method, such as Bi₂WO₆, and Bi₄O₅Br₂. For example, Ding et al. synthesized the h-BN/Bi₄O₅Br₂ via a facile micro emulsion/hydrothermal method with TX-100 as surfactant emulsion in Fig. 5 [97].

Hydrothermal method is also versatile for the application of 2D BN nanosheets coupled metal sulfides, such as BN/In₂S₃ [98], BN/CdS, BN/Cd_xZn_{1-x}S and BN/ZnIn₂S₄ [99]. For example, the BN/In₂S₃ composite was fabricated through one-pot hydrothermal method by heating a mixture of InCl₃·4H₂O and thiacetamide on the surface of BN nanosheet

[98]. Similarly, a simple hydrothermal method was also employed to obtain the a-BN/CdS [99]. Very recently, Gu et al. prepared 2D BN/g-C₃N₄ composite through a hydrothermal method, wherein a mixture of BN, NH₄Cl and g-C₃N₄ in water was heated for 12 h at 180 °C in an autoclave [100]. Solvothermal/hydrothermal methods were attractive to researchers owing to some advantages, such as mild reaction condition and simple control of reaction.

2.2.4. Thermal condensation process

Thermal condensation process is another method for preparation of semiconductor/BN composites. Sun et al. employed a thermal treatment to embed Pt NPs into hexagonal boron nitride (h-BN) layers [101]. The Pt@h-BN was synthesized by hydrogenation of NH₃BH₃ on the surface of Pt and then heated at 500 or 700 °C for 2 h in flowing NH₃. Similarly, this method can also be developed to encapsulate Ni NPs with few-layer h-BN shells. Gao et al. prepared the Ni@h-BN via the above method [102]. Firstly, a carbon support mixed with nickel nitrate (Ni(NO₃)₂) and boric acid (H₃BO₃) solutions was synthesized. Then, the mixture was heated in an autoclave at 120 °C. The obtained product was then annealed in NH₃ at different calcination time. From the XPS results, the graphitic h-BN shells can be synthesized through the reaction between H₃BO₃ and NH₃ at 700 °C.

Thermal condensation process was also employed to prepare the BCN composite. Qiu et al. fabricated the BCN via condensation [103]. Different amounts of BH₃NH₃ were doped into the classical carbon nitride condensation. Huang et al. introduced a novel and simple way of carbon doping of h-BN nanosheets to generate ternary BCN as sustainable and stable visible light photocatalysts [104]. They placed boron oxide, urea and a certain amount of glucose into the horizontal tube furnace. Thaweesak et al. prepared BCN via a one-step thermal condensation process [105]. BNH₆ was first mixed with dicyandiamide and NH₄Cl, and then transferred into alumina crucible at 600 °C for 4 h under N₂ flow.

2.2.5. Other techniques

Electrospinning approach has been used to fabricate BN based nanocomposites. Nasr et al. prepared the BN nanosheets/TiO₂ nanofibers via electrospinning technique [106]. They used different amounts of boron nitride and absolute ethanol as spun solution, and titanium tetrakisopropoxide ethanol mixed with polyvinylpyrrolidone as the precursor solution.

Microwave irradiation is a rapid and simple method to provide homogeneous heating process for synthesis of nanocrystals with controllable size and shape on the surface. It can be used for simultaneous formation of metal compounds and BN to prepare BN based hybrids. Boron nitride (BN)-modified bismuth oxychloride (BiOCl) materials have been synthesized via a facile microwave-assisted method [107]. Bi(NO₃)₃·5H₂O was first dispersed in glycerol solution, and a solution of NaCl was added dropwise. Then the mixture was transferred into a three-necked flask, and the reaction was carried out in microwave reactor at 1000 W and 140 °C for 1 h. This method could reduce the reaction time and greatly improve the efficiency of large-scale production.

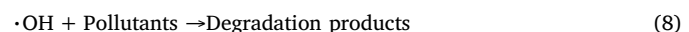
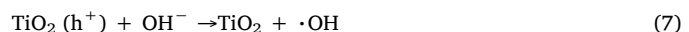
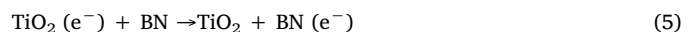
3. Semiconductor/BN composites in photocatalysis applications

In recent years, semiconductor photocatalysts have been expected to play an important role in solving many environmental and energy challenges. However, the fast recombination rates of photogenerated charge carriers caused the low efficiency, thus limiting its applications. Recently, semiconductor/BN composites have attracted extensive attention due to its well photocatalytic activity. The composites could potentially enhance the separating of electron-hole. Table 2 shows the applications of semiconductor/BN composites, which exhibit enhanced photocatalytic degradation of different target organic substrates. In addition, semiconductor/BN composites were also employed for H₂

evolution under light illumination.

3.1. Metal oxide/BN and metal sulfide/BN composites

Among metal oxide/BN semiconductor systems, TiO₂/BN composites were very attractive. TiO₂/BN composite was reported to have a high photocatalytic performance for the degradation of methylene blue (MB), methyl orange (MO) or rhodamine B (RhB). Mechanism revealed that the BN in the composites can promote charge separation and increase the adsorption of pollutants. Singh et al. revealed that the BN-TiO₂ showed an enhanced visible light photocatalytic activity for degradation of MB in water [108]. The photodegradation rate of BN-TiO₂ is 79% in 200 min, which is higher than that of TiO₂ (32%) in the visible region. MB molecules can be transferred from the solution to the surface of TiO₂ and adsorb with offset face-to-face orientation via π - π conjugation between MB and BN, and therefore, its adsorption ability of dyes increases compared to that of the pristine TiO₂. Fu et al. studied the performances of h-BN/TiO₂ for the degradation of RhB and MB under UV light irradiation [89]. The photocatalytic degradation rate of optimized h-BN/TiO₂ composite for RhB and MB was 15 and 8 times higher than the pristine TiO₂, respectively. Also, BN nanofiber was also combined with TiO₂ due to electrostatic attraction. The composite showed efficient photocatalytic decomposition of MO under UV light [106]. The removal rate constant for the optimized composite was reached 0.0586 min⁻¹, which showed 5 and 3.8 times higher than that of P25 and TiO₂ nanofiber alone. Si and co-workers prepared the few-atomic-layer BN hollow nanospheres for degradation of MO [109]. The shells of BN nanospheres only consist of 2–6 layers. In Fig. 6, the TEM and HRTEM image showed that the TiO₂ was dispersed on the surface of BN. The MO was completely degraded by the optimized composite in 12 min. The reaction mechanism (Eq. (4)–(8)) involved in h-BN/TiO₂ is given below:



BN/TiO₂ not only has a good photocatalytic activity under UV light but also has good photocatalytic property under visible light. Nitrogen-doped TiO₂ (TiO_{2-x}N_x)/BN was explored for visible light driven degradation of RhB [110]. Compared with pure TiO₂ and TiO_{2-x}N_x composite, the TiO_{2-x}N_x/BN composite exhibits much higher photocatalytic degradation activity. The degradation efficiency of RhB reaches 97.8% in 40 min. Gold nanoparticle-loaded TiO₂ (Au/TiO₂) as a visible light photocatalyst has attracted much attention. For example, Au/TiO₂/BN showed high photocatalytic activity towards the decomposition of crystal violet (CV) aqueous under solar light irradiation [76]. The apparent reaction rate constant for the optimized composite was estimated to be 10.3 $\mu\text{mol h}^{-1}$, which was higher than the pristine Au/TiO₂ (2.8 $\mu\text{mol h}^{-1}$). The role of BN in the Au/TiO₂/BN composite is to promote charge separation in TiO₂ and improve the adsorption ability of CV. Recently, Liu et al. demonstrated that the porous BN/TiO₂ hybrid was highly active for the degradation of RhB under visible light [77]. The porous BN/TiO₂ hybrid nanosheets (38 wt%) achieve a degradation percentage up to 99% within 6 h, which is much higher than that of P25 (60%).

Except TiO₂, other metal oxide (SnO₂, WO₃, ZnO, etc) photocatalyst and its modified materials also have many potential applications in photocatalysis. BN with its large surface area can serve as a good adsorbent to gather pollutants around the semiconductor particles [111]. Moreover, fabrication of heterojunction with BN is beneficial for enhancing them separation of electron-hole pairs. Wang et al. evaluated

Table 2

Summary of the photocatalytic properties of BN based photocatalysts toward pollutant degradation.

Photocatalyst	Synthesis method	BN content	Pollutants	Photocatalytic activity	Enhancement factor	Reference
BN-TiO ₂	In-situ grown	44%	MB	0.002 min ⁻¹	2 times than TiO ₂	[108]
BN/TiO ₂	Electro spinning	10 wt%	MO	0.0586 min ⁻¹	3.8 times than TiO ₂	[106]
h-BN/TiO ₂	Ball milling	0.5 wt%	RhB and MB	0.134 min ⁻¹ , and 0.063 min ⁻¹	15 and 8 times than TiO ₂	[89]
TiO ₂ @BN	In-situ grown	80	MO	12 min in 90%	12 min in 20% for TiO ₂	[109]
SnO ₂ /BN	In-situ grown	20 wt%	MO	30 min in 92%	30 min in 21.6% for SnO ₂ /Al ₂ O ₃	[78]
BN/WO ₃	Calcination	5 wt %	RhB	0.6327 h ⁻¹	2.8 times than WO ₃	[110]
h-BN/ZnO	Ball milling	1.0 wt%	RhB, MB	20 min in 82%, 20 min in 60%	20 min in 33%, 20 min 30% in ZnO	[90]
TiO ₂ – _x N _x /BN	Hydrolytic precipitation	25%	RhB	0.0986 min ⁻¹	–	[111]
h-BN/TiO ₂	Thermal recrystallization	38 wt%	RhB	6 h in 99%	6 h in 60% for P25	[77]
BN/Ag ₃ PO ₄	Precipitation	0.5 wt%	RhB	0.28 min ⁻¹	3 times than Ag ₃ PO ₄	[82]
BN/AgBr	Precipitation	2 wt%	MO	0.11068 min ⁻¹	1.8 times than AgBr	[83]
AgI/BN	Precipitation	0.2 wt%	RhB	0.04596 min ⁻¹	1.86 times than AgI	[79]
BN/AgBr/AgI	Precipitation	3 wt%	RhB and MO	0.568 min ⁻¹ for RhB, 0.525 min ⁻¹ for MO	4.96 times and 3.69 times higher than that of AgBr	[80]
h-BN/Ag ₃ VO ₄	Precipitation	3 wt%	RhB	0.0384 min ⁻¹	6.2 times than Ag ₃ VO ₄	[86]
BN/Ag ₂ CO ₃	Precipitation	3 wt%	RhB	0.05919 min ⁻¹	1.24 times higher than pure Ag ₂ CO ₃	[85]
Ag ₂ CrO ₄ /BNNS	Precipitation	10 wt%	RhB	0.02769 min ⁻¹	1.5 times than Ag ₂ CrO ₄	[84]
BN/BiOI	Solvothermal	0.5 wt%	RhB	0.02291 min ⁻¹	2.1 times than BiOI	[96]
BN/BiOBr	Solvothermal	1 wt%	RhB, CIP	30 min in 99% RhB, 80 min in 81.5% CIP	30 min in 30%, 80 min in 57.3% for BiOBr	[94]
h-BN/Bi ₄ O ₅ Br ₂	Micro emulsion/hydrothermal	1 wt%	PTBP	0.02 min ⁻¹	4 times than Bi ₄ O ₅ Br ₂	[97]
BN/Bi ₄ O ₅ I ₂	Ionic liquid assisted solvothermal	3 wt%	BPA	20 min in 97%	20 min in 57% of Bi ₄ O ₅ I ₂	[112]
BN/Bi ₂ WO ₆	Hydrothermal	3 wt%	RhB	0.0435 min ⁻¹	2.4 times than Bi ₂ WO ₆	[113]
SnS ₂ /FBNNS	Hydrothermal	10 wt%	RhB	0.01268 min ⁻¹	3.8 times than SnS ₂	[114]
2D BN/g-C ₃ N ₄	Hydrothermal	0.5 wt%	RhB	0.0286 min ⁻¹	5.41 times than g-C ₃ N ₄	[100]
h-BN/g-C ₃ N ₄	In-situ direct growth	0.48%	RhB, TC	0.13091 min ⁻¹ , 0.02775 min ⁻¹	7.3 and 2.3 times than that of pure g-C ₃ N ₄ respectively	[115]
BN/BiPO ₄	Solvothermal	1 wt%	ENR	0.0190 min ⁻¹	1.74 times than BiPO ₄	[93]

the visible light photocatalytic activity of SnO₂/BN for degradation of methyl orange (MO) in water [78]. The degradation efficiency of MO by SnO₂/BNMB reached 92% after 30 min under visible light irradiation, whereas the pure SnO₂ was inactive for the degradation of MO. The improved photocatalytic activity of SnO₂/BNMB was because the optical absorption of SnO₂ and the strong adsorption ability of the support h-BN. A similar mechanism has also been put forward for RhB degradation over BN/WO₃ under visible light irradiation [112]. Xu et al. reported the BN/WO₃ composite as a visible light photocatalyst. The hybrid composite exhibited enhanced photodegradation efficiency for RhB. The apparent reaction of the composite was estimated to be 0.6327 h⁻¹, which was 2.8 times higher than the pure WO₃. Fu et al. found that the photocatalytic activity of ZnO can be also improved by coupling with h-BN [90]. For h-BN (1.0 wt%)/ZnO, the degradation efficiencies of RhB and MB reach to 82% and 60% under 20 min irradiation, respectively. While the corresponding degradation efficiencies are 33% and 30% for pure ZnO, respectively. The enhancement activity of h-BN/ZnO is attributed to the negatively charged h-BN surface, which can promote the transfer of the photoinduced holes to ZnO surface and facilitate the adsorption of cationic dyes around ZnO.

Metal sulfide semiconductors have attracted tremendous attention owing to their superior electrical and optical properties. CdS, as one of the narrow bandgap semiconductors (2.2–2.4 eV), exhibits high optical response and has been widely applied as a photoharvester for photocatalysis. However, the photocorrosion effect makes CdS unstable as a photocatalyst thereby greatly limited its practical application. CdS can be combined with BN to assemble CdS/BN composite for H₂ evolution. For example, Zhang and co-workers fabricated the ternary Pt/BN/CdS composites for visible light driven H₂ production from water [91]. For the composite with 5.0 wt% BN, the evolution rate of H₂ can be reached as high as 17.56 mmol g⁻¹ h⁻¹ which was about 3 times higher compared with the Pt/CdS. The heterojunction between BN and CdS was important for the separation of photogenerated charge carriers, this effect can be enhanced the photocatalytic activity of BN/CdS. Lately, Ma et al. fabricated CdS/hexagonal boron nitride nanosheets (BNNSS) and applied it to hydrogen evolution [113]. The rate of H₂ evolution on

0.5 wt% CdS/BNNSS was 439.4 $\mu\text{mol g}^{-1} \text{h}^{-1}$, which was 2.3 times higher than that of the pure CdS. It can be found that the rate of H₂ evolution on Pt/CdS/BNNSS was 5.961 mmol g⁻¹ h⁻¹ when Pt was loaded. BNNSS were inactive for H₂ evolution, but it can offer a large surface for catalytic reaction. In addition, the well connection of BN and CdS broaden the photo-absorption region and enhance electronic communication of CdS, which make the enhancement of photocatalytic H₂ evolution.

3.2. Silver based semiconductor/BN composites

Recently, silver based semiconductors exhibit promising photocatalytic activity for the water splitting and removal of organic pollutants. BN can be coupled with the silver based semiconductor for the enhancement of photocatalytic activity. Ag₃PO₄ has high photo-oxidative activity under visible light irradiation but it is susceptible to corrosion. Zhu et al. constructed the BN/Ag₃PO₄ for MB degradation under visible light irradiation [114]. The degradation rate constant of MB by 1% BN/Ag₃PO₄ was about 2.79 times higher than that of pure Ag₃PO₄. The excellent photocatalytic activity of BN/Ag₃PO₄ was ascribed to the high separation efficiency of photogenerated electrons between the BN and Ag₃PO₄. The superior electron-hole separation efficiency of BN/Ag₃PO₄ was examined by photoluminescence spectra, electrochemical impedance spectroscopy and transient photocurrent responses experiments. A similar mechanism was also obtained by h-BN/Ag₃VO₄, BN/Ag₂CO₃ and Ag₂CrO₄/FBNNS [84]. Lv et al. reported the RhB photocatalytic degradation rate constant of h-BN/Ag₃VO₄ was 0.0384 min⁻¹, which was about 6 folds that of pure Ag₃VO₄ (0.0062 min⁻¹) [86]. Also, the results of RhB degradation showed that the removal rate of 3 wt% BN/Ag₂CO₃ was almost 1.24 times higher than pure Ag₂CO₃ under visible light irradiation [85].

Silver halides (e.g., AgBr and AgI) are well known as photosensitive materials in photography and display high photocatalytic activity. Coupling BN with silver halides to form composites, such as BN/AgBr, AgI/BN and AgI/AgBr/h-BN have been found to be enhanced the photocatalytic activity of bulk material [83]. Choi et al. studied the

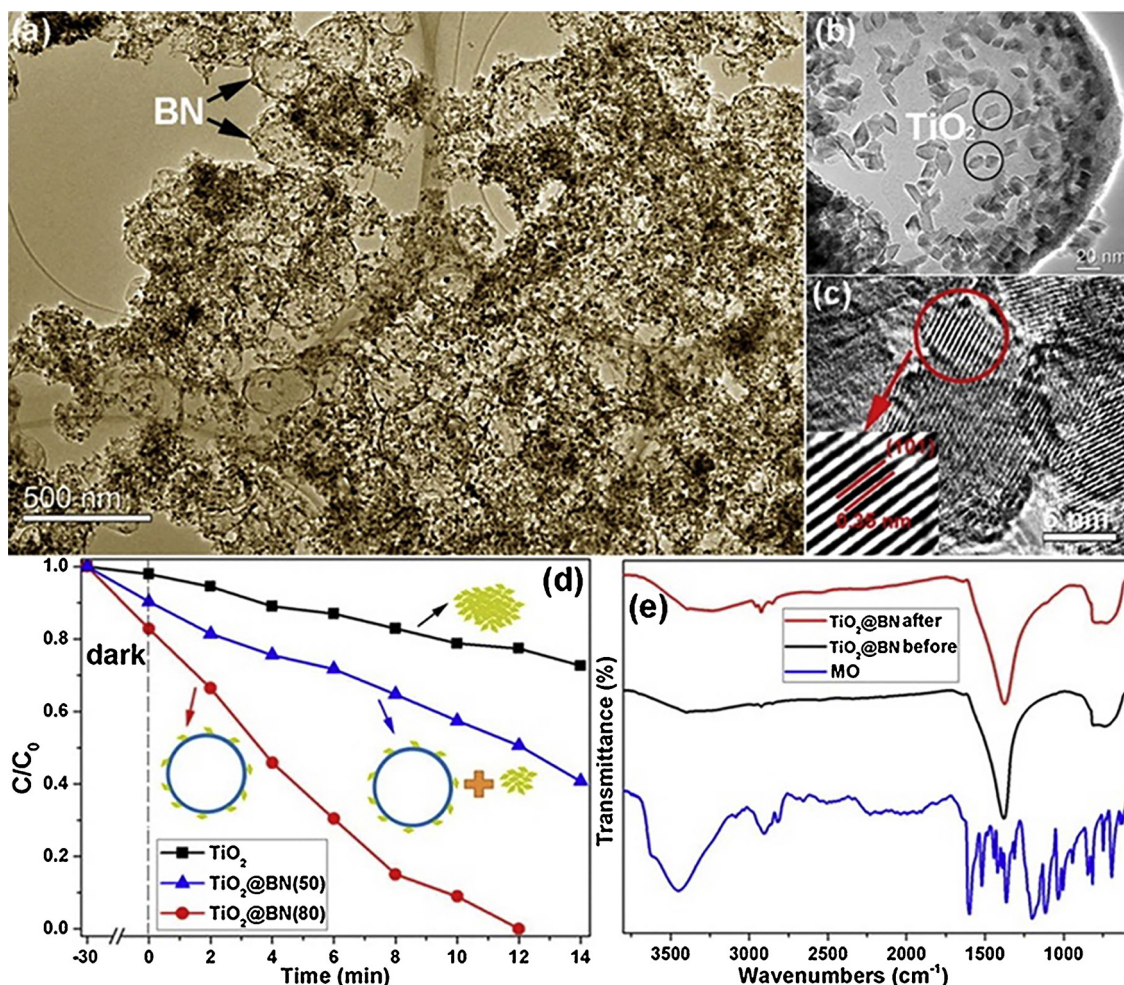


Fig. 6. (a, b) TEM images of TiO₂@BN(80) hollow nanospheres hybrid. (c) HRTEM image of TiO₂ NCs. Inset shows the magnified interplanar spaces of TiO₂ labeled. (d) Photocatalytic degradation curves of MO with BN, TiO₂ NCs, TiO₂@BN(50), and TiO₂@BN(80). (e) FTIR spectra of MO, TiO₂@BN hybrids before and after reaction. Reproduced with permission from Ref. [109]. Copyright 2017, ACS.

effectiveness of BN/AgI composite for the decomposition of RhB under visible light irradiation [79]. The 0.2 wt% BN/AgI composite exhibited a significantly higher activity than that of the bare AgI. Moreover, the composite exhibited good photostability, which showed a degradation efficiency of 87.8% after 5 successive experimental runs. This enhanced photoactivity and stability of AgI/BN may be attributed to the effect of heterojunction between AgI and BN. On the basis of BN/AgI, Wu et al. constructed the heterostructured AgI/AgBr/h-BN composite for degradation RhB and MO [80]. The formation of AgI/AgBr navy beans could promote the separation of photogenerated electron-hole pairs. Under visible light irradiation, the photocatalytic activity was in the order AgI/AgBr/h-BN > AgI/AgBr > AgBr. The photogenerated electron of AgI could be injected into the CB edge of AgBr, and then the electrons could be effectively transferred to the surface of h-BN and further could be turned into superoxide radical on the surface of the catalyst.

3.3. Bismuth-based semiconductor/BN composites

Bismuth based semiconductors such as BiOX (X = Br, Cl and I) [94,96], Bi₄O₅I₂ [115], Bi₄O₅Br₂ [97], Bi₂WO₆ [116] and BiPO₄ [93] have emerged as attractive materials in various photocatalytic applications. Bismuth based semiconductors were also demonstrated for integration with BN for photocatalytic degradation of organic pollutants. When 0.5 wt% BN was loaded in BiOI, a significant improvement of the photodegradation activity of RhB could be observed to contribute

to the performance by a factor of 2. The results were presented in Fig. 7a and b [96]. The heterojunction mechanism between the BN and BiOI was proposed for the improved activity. Similar to BiOI, BiOBr was also proven to conjugate with BN for photocatalytic degradation. Di and co-worker demonstrated that the 1 wt% BN/BiOBr composite presented enhancement for the photodegradation of RhB, ciprofloxacin (CIP), and tetracycline hydrochloride (TC) under visible light driven [94]. As shown in Fig. 7c and 7d, nearly 81.5% of CIP was degraded after 90 min by 1 wt% BN/BiOBr, while only 57.3% degradation was achieved by pure BiOBr. The variation in photocatalytic efficiency was attributed to the improved visible light harvesting ability and high separation efficiency of photogenerated electron-hole pairs. In addition, Ding et al. construct the heterojunction photocatalyst h-BN/Bi₄O₅Br₂ for degradation 4-tert-Butylphenol (PTBP) [117]. The optimum amount of loaded h-BN is 1 wt%, and the photodegradation followed first-order kinetics with a reaction rate constant of 0.02 min⁻¹, which was 4 times larger than that of the pure Bi₄O₅Br₂. As shown in Fig. 8a-e, density functional theory (DFT) calculations revealed that h-BN/Bi₄O₅Br₂ would reduce the hybrid electron density of h-BN in the CB, and thus the CB electrons of h-BN migrate to the surface of Bi₄O₅Br₂, preventing recombination of electron-hole pairs.

In contrast to organic pollutants, inorganic metal ions are problematic since they are not biodegradable and endanger the living organisms. Hexavalent chromium (Cr⁶⁺) is a common pollutant from mining industry and electroplating industry, which is a significant threat to human health. In contrast, Cr³⁺ is an essential trace element

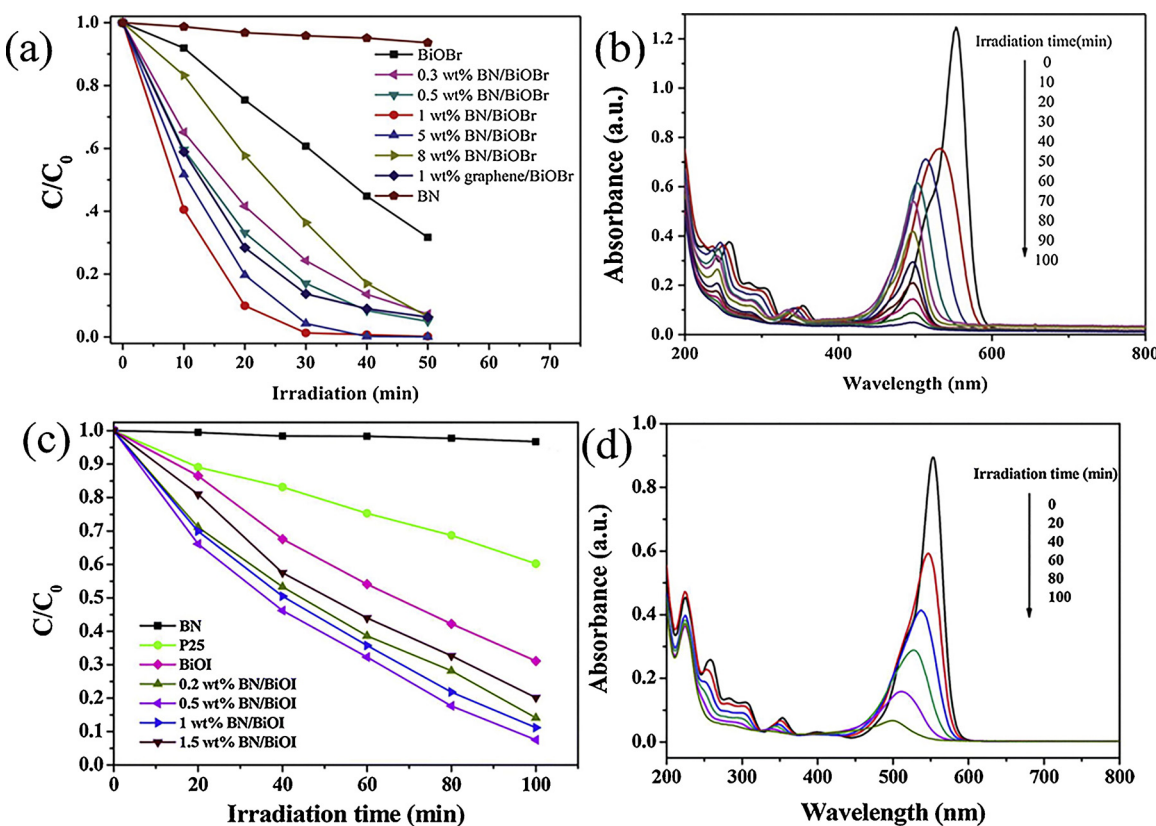
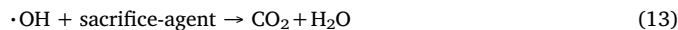
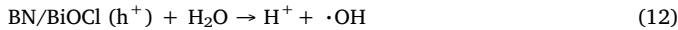
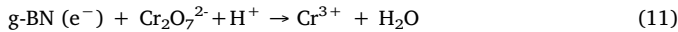
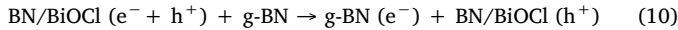
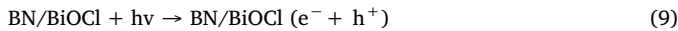


Fig. 7. (a) Photodegradation of RhB by BiOBr and graphene-like BN/BiOBr composites under visible light irradiation; (b) time-dependent UV-vis absorption spectra in the presence of 1 wt% graphene-like BN/BiOBr. (c) Photodegradation of RhB by BiOI and graphene-like BN/BiOI composites under visible light irradiation. (d) Variations in the characteristic absorption of RhB under visible light irradiation using 0.5 wt% BN/BiOI. (a–b) Reproduced with permission from Ref. [96]. Copyright 2016, Elsevier. (c–d) Reproduced with permission from Ref. [94]. Copyright 2017, Elsevier.

and required for human health. Hence, reduction of Cr^{6+} to Cr^{3+} is an effective method of controlling its pollution. Photocatalytic reduction is considered as a promising method owing to its low cost and environmental friendly [118]. Xu et al. studied the photoactivity of g-BN-decorated BiOCl microspheres for Cr^{6+} reduction upon visible-light irradiation [118]. The prepared 1% BN/BiOCl materials exhibited an up to 2.03-fold enhanced Cr^{6+} reduction rate constant compared with pure BiOCl microspheres due to the suppressed recombination of photo-generated electron–hole pairs. The mechanism was presented in the following equations (Eq. (9)–(13)). Also, Xie et al. reported TiO_2 /P-BNNs showed an enhanced photocatalytic activity for simultaneous removal of dyes (Lanaset Red50, LR2B) and Cr^{6+} [119].



3.4. $\text{g-C}_3\text{N}_4$ /BN composites

Metal free photocatalyst graphene carbon nitride ($\text{g-C}_3\text{N}_4$) was proposed by Wang et al. in 2009 [120]. The band gap of $\text{g-C}_3\text{N}_4$ was 2.5–2.7 eV [121,122]. The few-layer BN nanosheets were well-attached to the $\text{g-C}_3\text{N}_4$ to establish sufficient contact interface in the 2D/2D construction between the two materials. Gu et al. introduced the BN on the surface of $\text{g-C}_3\text{N}_4$ to form the nanocomposite in Fig. 9a [100]. The optimized 0.5% BN/ $\text{g-C}_3\text{N}_4$ sample presented the highest photocatalytic

activity towards RhB degradation, which can achieve the high efficiency of 98.2% within 120 min. Recently, our group also reported that the 0.48% h-BN/ $\text{g-C}_3\text{N}_4$ (denoted as BC-3) nanocomposites showed higher photocatalytic activity towards RhB and TC degradation compared to $\text{g-C}_3\text{N}_4$ [123]. It was observed that 99.5% of RhB was decomposed in 40 min, while 80.5% of TC was degraded after 1 h over BC-3. The superior photocatalytic activity of h-BN/ $\text{g-C}_3\text{N}_4$ composites could be caused by the larger surface area and higher separation efficiency of electron–hole pairs. The degradation mechanism was proposed in Fig. 9b.

Loading $\text{g-C}_3\text{N}_4$ on h-BN sheets can also improve the photocatalytic activity for the H_2 evolution. For example, He et al. successfully demonstrated the enhanced photocatalytic activity of CN/h-BN (CBN-x) for the H_2 production [57]. Fig. 10a shows that the CBN-6 was composed of 4–6 layers and has a porous structure. The HRTEM image revealed the layered CN was formed on h-BN surface (Fig. 10b). It was found that CBN-6 is more effective than BN for the photocatalytic H_2 evolution (Fig. 10c). The band gap of CBN is gradually reduced by loading of CN (Fig. 10d). In such system, the photogenerated electrons of CN could transfer to the conduction band of BN, while the holes of BN are transferred into the CN phase to achieve better charge separation and prolong the lifetime of the electrons.

4. Role of BN in semiconductor/BN composites

BN can accept photogenerated electrons from the CB of most semiconductors, which will efficiently suppress the recombination of photogenerated charges and enhance their photocatalytic degradation activity. The role of BN as an electron acceptor and transporter has been extensively discussed. For example, when the h-BN was coupled with Ag_3VO_4 , the electrons in Ag_3VO_4 could transfer to the h-BN for the

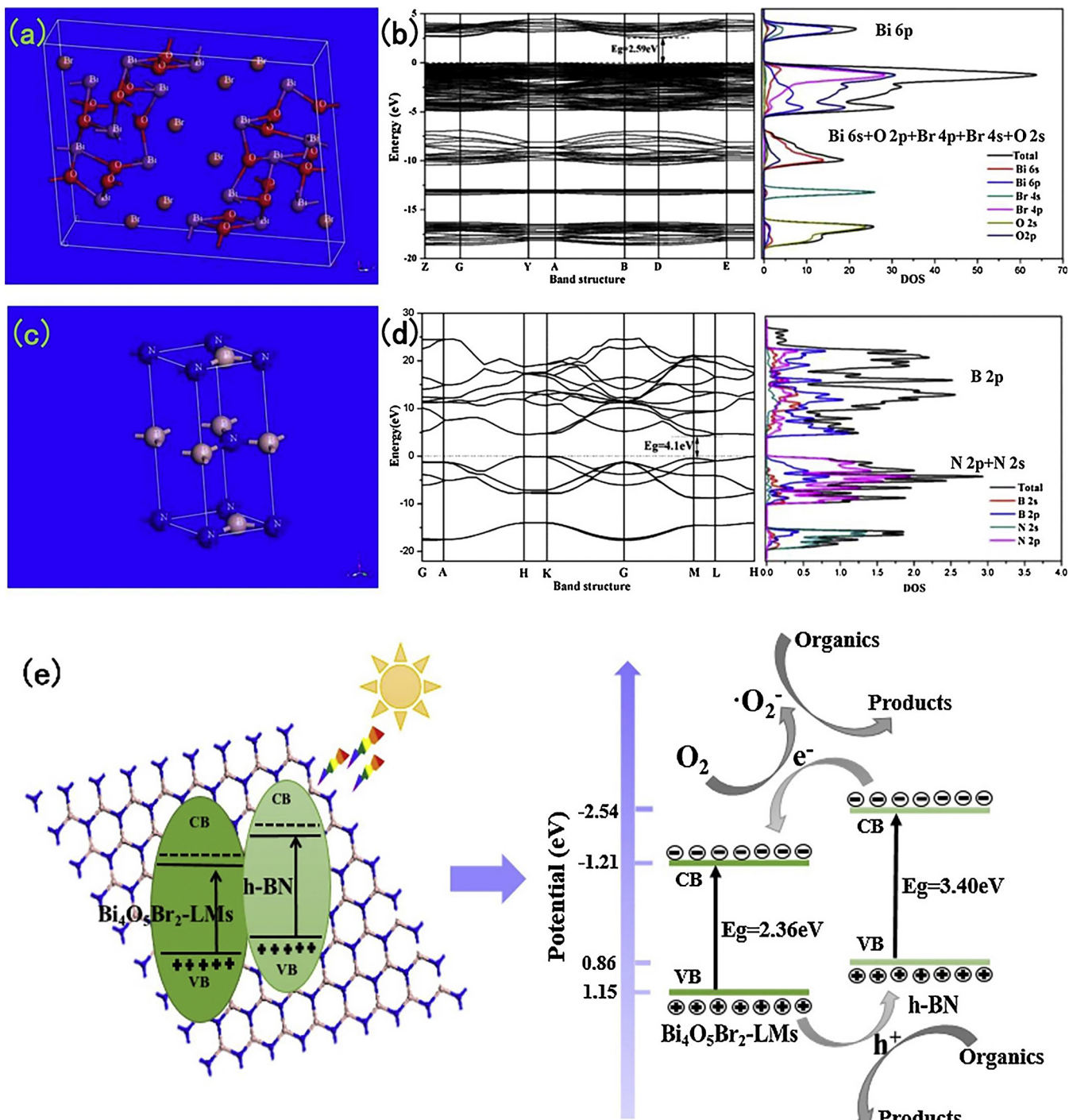


Fig. 8. Crystal structures, calculated band structures and density of states of (a, b) $\text{Bi}_4\text{O}_5\text{Br}_2$ and (c, d) h-BN. (e) Schematic of the separation and transportation of photo-induced charges in the h-BN/ $\text{Bi}_4\text{O}_5\text{Br}_2$ composites combined with the possible photocatalytic degradation mechanism. Reproduced with permission from Ref. [117]. Copyright 2017, Elsevier.

interfacial interaction between BN and Ag_3VO_4 and resulted in effective separation of charge carriers [86]. Therefore, the BN modification will lead the improved photocatalytic activity of semiconductor/BN.

Moreover, it has been found that the ball-milled h-BN can be used as holes transfer promoter for semiconductors, such as TiO_2 , ZnO and CdS [89–91]. When the semiconductor and BN contacted, the holes from semiconductor could transfer to the surface due to the negatively charged of BN. For example, h-BN/ TiO_2 composite photocatalyst was prepared by ball milling process. The transfer rate of holes from the bulk of TiO_2 to its surface can be improved by the negatively charged h-

BN. The efficient holes transfer from TiO_2 to the BN resulted in the enhancement of photocatalytic activity of TiO_2 .

Furthermore, porous BN has high surface area and good thermal stability. It could be used as a support material for semiconductors to enhance the photocatalytic activity [77,92]. For porous BN/ TiO_2 composite, the high BET surface area contributed to their high adsorption ability for pollutant [124]. It is important to enhance adsorption ability of a photocatalyst because the photo-induced reaction species are located on its surfaces mostly. In addition, the large surface area of porous BN provides a good spatial condition for the charge

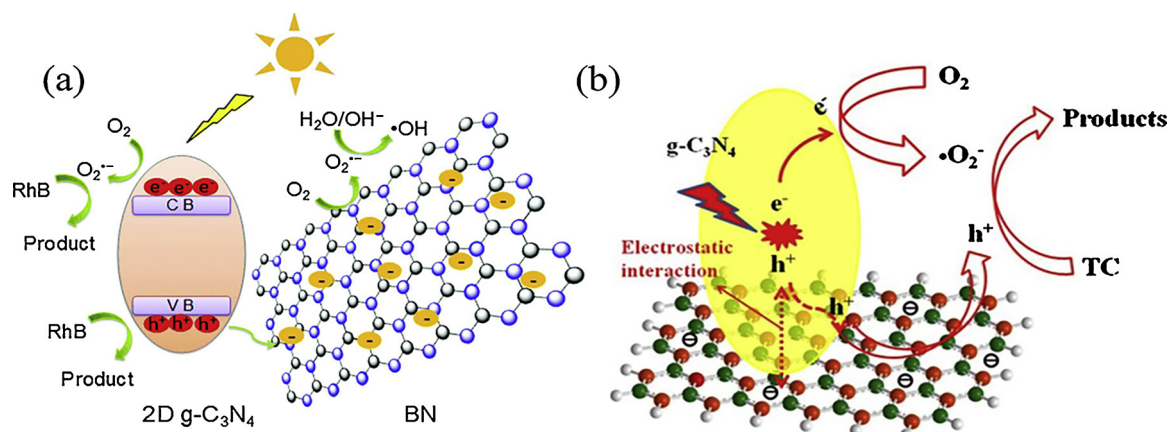


Fig. 9. Possible photocatalytic mechanism of RhB (a) and TC (b) degradation by 2D BN/g-C₃N₄. (a) Reproduced with permission from Ref. [100]. Copyright 2017, Elsevier. (b) Reproduced with permission from Ref. [123]. Copyright 2018, Elsevier.

transportation, thus ensuring a continuous charge transfer.

5. Conclusions and perspective

In conclusion, this work summarized recent progress on the synthesis of BN and semiconductor/BN composites. The BN can be introduced into various semiconductor photocatalysts to form semiconductor/BN composites. Many methods including *in-situ* growth method, ball milling method, hydrothermal and solvothermal method,

and thermal condensation method have been explored for the syntheses of the semiconductor/BN composites. These semiconductor/BN composites have various applications in photocatalytic fields, such as pollutant degradation and photocatalytic hydrogen evolution. Coupling BN with semiconductors can improve the photocatalytic activity of semiconductors dramatically. In addition, the role of BN in semiconductor/BN composites is discussed in depth.

Despite the bright future of BN-based materials, there are some issues that should be taken into consideration:

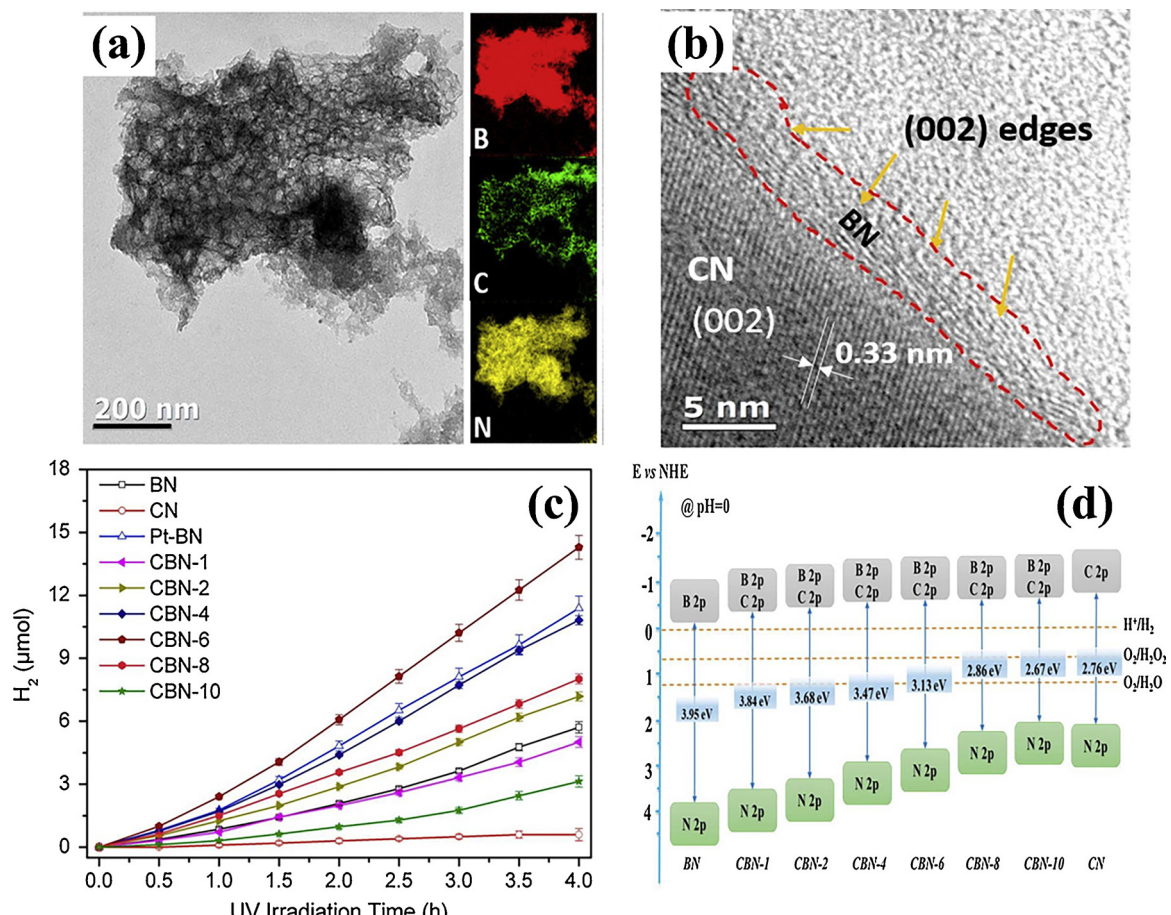


Fig. 10. (a-b) TEM images and EELS mapping data of CBN-6, (c) Time profiles of photocatalytic H₂ production in the presence of BN, CN or CBN-x samples. (d) Determined band energy levels of CBN-x electrodes, in comparison with pure *h*-BN and CN electrodes. The standard reduction potentials for H⁺/H₂, O₂/H₂O₂ and O₂/H₂O couples are shown as a reference. Reproduced with permission from Ref. [57]. Copyright 2017, Elsevier.

(1) Preparation of BN and BN-based nanomaterials. The preparation methods of functionalized BN and BN-based nanomaterials are still rather difficult, particularly compared to graphene analogues. This situation is primarily explained by high chemical inertness of BN-based materials that prevent them from direct modifications. A lot of synthetic methods were applied for the preparation of modified BN and BN-based nanomaterials, however, the yield and efficiency of these methods are not satisfied yet.

(2) Roles of BN. The roles of BN were reviewed, while it is far from completion. It is reported that the strong interaction between BN and semiconductor improves the charge separation and transfer properties in the BN-based photocatalysts. BN can promote the immigration of holes from the bulk of photocatalyst to its surface and consequently improve the photocatalytic activity. Bonds like B–O–Ti have been formed in the BN/TiO₂. The semiconductors properties of BN are usually overlooked. Besides, the structure of BN plays a crucial role in BN/semiconductor hybrids. 0D BN quantum dots, 1D BN nanorods and 3D BN framework have special electronic and optical properties, which are different from 2D BN nanosheet. The unique properties of BN QDs might be beneficial to separation of photoinduced charges and absorption of solar light.

(3) Theoretical calculation of BN-based materials. Many experiments demonstrated the key roles of BN in the enhancement of photocatalytic activity. However, the inherent mechanism in the enhancement of photocatalytic activity has not been figured out yet. Theoretical calculations can simulate the electronic properties and the photogenerated charge carriers at the molecular level of BN based photocatalysts, which are beneficial to give an overall understanding of the experimental results.

Acknowledgements

This study was financially supported by the Program for the National Natural Science Foundation of China (51579098, 51779090, 51709101, 51278176, 51521006, 51378190, 51408206, 51508177), the National Program for Support of Top-Notch Young Professionals of China (2014), the Fundamental Research Funds for the Central Universities, Hunan Provincial Science and Technology Plan Project (No. 2016RS3026, 2017SK2243), the Program for Changjiang Scholars and Innovative Research Team in University (IRT-13R17), and the Fundamental Research Funds for the Central Universities (531107050978, 531107051080).

References

- J. Liang, Z. Yang, L. Tang, G. Zeng, M. Yu, X. Li, H. Wu, Y. Qian, X. Li, Y. Luo, *Chemosphere* 181 (2017) 281–288.
- H. Wu, C. Lai, G. Zeng, J. Liang, J. Chen, J. Xu, J. Dai, X. Li, J. Liu, M. Chen, L. Lu, L. Hu, J. Wan, *Crit. Rev. Biotechnol.* 37 (2017) 754–764.
- Y. Zhang, G.M. Zeng, L. Tang, J. Chen, Y. Zhu, X.X. He, Y. He, *Anal. Chem.* 87 (2015) 989–996.
- J. Wan, G. Zeng, D. Huang, L. Hu, P. Xu, C. Huang, R. Deng, W. Xue, C. Lai, C. Zhou, K. Zheng, X. Ren, X. Gong, J. Hazard. Mater. 343 (2018) 332–339.
- W. Xiong, J. Tong, Z. Yang, G. Zeng, Y. Zhou, D. Wang, P. Song, R. Xu, C. Zhang, M. Cheng, *J. Colloid Interface Sci.* 493 (2017) 17–23.
- C. Zhou, C. Lai, P. Xu, G. Zeng, D. Huang, C. Zhang, M. Cheng, L. Hu, J. Wan, Y. Liu, W. Xiong, Y. Deng, M. Wen, *ACS Sustain. Chem. Eng.* 6 (2018) 4174–4184.
- M. Cheng, G. Zeng, D. Huang, C. Yang, C. Lai, C. Zhang, Y. Liu, *Chem. Eng. J.* 314 (2017) 98–113.
- S. Zhong, C. Zhou, X. Zhang, H. Zhou, H. Li, X. Zhu, Y. Wang, J. Hazard. Mater. 276 (2014) 58–65.
- P. Xu, G.M. Zeng, D.L. Huang, C.L. Feng, S. Hu, M.H. Zhao, C. Lai, Z. Wei, C. Huang, G.X. Xie, *Sci. Total Environ.* 424 (2012) 1–10.
- C. Zhou, C. Lai, P. Xu, G. Zeng, D. Huang, Z. Li, C. Zhang, M. Cheng, L. Hu, J. Wan, F. Chen, W. Xiong, R. Deng, *ACS Sustain. Chem. Eng.* 6 (2018) 6941–6949.
- X. Tan, Y. Liu, G. Zeng, X. Wang, X. Hu, Y. Gu, Z. Yang, *Chemosphere* 125 (2015) 70–85.
- J.-H. Deng, X.-R. Zhang, G.-M. Zeng, J.-L. Gong, Q.-Y. Niu, J. Liang, *Chem. Eng. J.* 226 (2013) 189–200.
- M. Chen, P. Xu, G. Zeng, C. Yang, D. Huang, J. Zhang, *Biotechnol. Adv.* 33 (2015) 745–755.
- C. Zhang, C. Lai, G. Zeng, D. Huang, L. Tang, C. Yang, Y. Zhou, L. Qin, M. Cheng, *Biosens. Bioelectron.* 81 (2016) 61–67.
- F. Long, J.-L. Gong, G.-M. Zeng, L. Chen, X.-Y. Wang, J.-H. Deng, Q.-Y. Niu, H.-Y. Zhang, X.-R. Zhang, *Chem. Eng. J.* 171 (2011) 448–455.
- P. Xu, G.M. Zeng, D.L. Huang, C. Lai, M.H. Zhao, Z. Wei, N.J. Li, C. Huang, G.X. Xie, *Chem. Eng. J.* 203 (2012) 423–431.
- X. Ren, G. Zeng, L. Tang, J. Wang, J. Wan, Y. Liu, J. Yu, H. Yi, S. Ye, R. Deng, *Sci. Total Environ.* 610 (2018) 1154–1163.
- D.-L. Huang, R.-Z. Wang, Y.-G. Liu, G.-M. Zeng, C. Lai, P. Xu, B.-A. Lu, J.-J. Xu, C. Wang, C. Huang, *Environ. Sci. Pollut. Res.* 22 (2015) 963–977.
- D. Huang, L. Liu, G. Zeng, P. Xu, C. Huang, L. Deng, R. Wang, J. Wan, *Chemosphere* 174 (2017) 545–553.
- L. Hu, J. Wan, G. Zeng, A. Chen, G. Chen, Z. Huang, K. He, M. Cheng, C. Zhou, W. Xiong, C. Lai, P. Xu, *Environ. Sci. Nano* 4 (2017) 2018–2029.
- M. Cheng, G. Zeng, D. Huang, C. Lai, P. Xu, C. Zhang, Y. Liu, *Chem. Eng. J.* 284 (2016) 582–598.
- C. Zhang, C. Lai, G. Zeng, D. Huang, C. Yang, Y. Wang, Y. Zhou, M. Cheng, *Water Res.* 95 (2016) 103–112.
- M. Cheng, G. Zeng, D. Huang, C. Lai, P. Xu, C. Zhang, Y. Liu, J. Wan, X. Gong, Y. Zhu, J. Hazard. Mater. 312 (2016) 184–191.
- D. Huang, X. Gong, Y. Liu, G. Zeng, C. Lai, H. Bashir, L. Zhou, D. Wang, P. Xu, M. Cheng, *Planta* (2017) 1–11.
- J.-L. Gong, B. Wang, G.-M. Zeng, C.-P. Yang, C.-G. Niu, Q.-Y. Niu, W.-J. Zhou, Y. Liang, J. Hazard. Mater. 164 (2009) 1517–1522.
- X. Li, J. Yu, S. Wageh, A.A. Al-Ghamdi, J. Xie, *Small* 12 (2016) 6640–6696.
- D. Huang, X. Wang, C. Zhang, G. Zeng, Z. Peng, J. Zhou, M. Cheng, R. Wang, Z. Hu, X. Qin, *Chemosphere* 186 (2017) 414–421.
- J. Wang, Z. Yang, X. Gao, W. Yao, W. Wei, X. Chen, R. Zong, Y. Zhu, *Appl. Catal. B: Environ.* 217 (2017) 169–180.
- X. Chen, Q. Chen, W. Jiang, Z. Wei, Y. Zhu, *Appl. Catal. B: Environ.* 211 (2017) 106–113.
- C. Lai, M.-W. Wang, G.-M. Zeng, Y.-G. Liu, D.-L. Huang, C. Zhang, R.-Z. Wang, P. Xu, M. Cheng, C. Huang, *Appl. Surf. Sci.* 390 (2016) 368–376.
- W. Chen, Y.-X. Hua, Y. Wang, T. Huang, T.-Y. Liu, X.-H. Liu, *J. Catal.* 349 (2017) 8–18.
- C.Y. Zhou, C. Lai, D.L. Huang, G.M. Zeng, C. Zhang, M. Cheng, L. Hu, J. Wan, W.P. Xiong, M. Wen, X.F. Wen, L. Qin, *Appl. Catal. B: Environ.* 220 (2018) 202–210.
- G. Mamba, A.K. Mishra, *Appl. Catal. B: Environ.* 198 (2016) 347–377.
- L. Jiang, X. Yuan, Y. Pan, J. Liang, G. Zeng, Z. Wu, H. Wang, *Appl. Catal. B: Environ.* 217 (2017) 388–406.
- M. Zhang, W. Jiang, D. Liu, J. Wang, Y. Liu, Y. Zhu, Y. Zhu, *Appl. Catal. B: Environ.* 183 (2016) 263–268.
- Q. Zheng, D.P. Durkin, J.E. Elenewski, Y. Sun, N.A. Banek, L. Hua, H. Chen, M.J. Wagner, W. Zhang, D. Shuai, *Environ. Sci. Technol.* 50 (2016) 12938–12948.
- X. An, J.C. Yu, *Rsc Adv.* 1 (2011) 1426.
- Q. Xiang, J. Yu, M. Jaroniec, *Chem. Soc. Rev.* 41 (2012) 782–796.
- M. Yankowitz, K. Watanabe, T. Taniguchi, P. San-Jose, B.J. LeRoy, *Nat. Commun.* 7 (2016) 13168.
- C. Huang, C. Li, G. Shi, *Energy Environ. Sci.* 5 (2012) 8848.
- X.-F. Jiang, Q. Weng, X.-B. Wang, X. Li, J. Zhang, D. Golberg, Y. Bando, J. Mater. Sci. Technol. 31 (2015) 589–598.
- J. Wang, Y. Wu, Y. Xue, D. Liu, X. Wang, X. Hu, Y. Bando, W. Lei, J. Mater. Chem. A 6 (2018) 1363–1369.
- Z. Zhang, E.S. Penev, B.I. Yakobson, *Chem. Soc. Rev.* 46 (2017) 6746–6763.
- W. Peiwen, Y. Shize, Z. Wenshuai, L. Hongping, C. Yanhong, Z. Huiyuan, L. Huaming, D. Sheng, *Small* 13 (2017) 1701857.
- G. Xie, K. Zhang, B. Guo, Q. Liu, L. Fang, J.R. Gong, *Adv. Mater.* 25 (2013) 3820–3839.
- J. Wang, J. Hao, D. Liu, S. Qin, C. Chen, C. Yang, Y. Liu, T. Yang, Y. Fan, Y. Chen, *Nanoscale* 9 (2017) 9787–9791.
- D. Liu, W. Lei, S. Qin, Y. Chen, *Sci. Rep.* 4 (2014) 4453.
- L. Weiwei, L. Dan, C. Ying, *Adv. Mater. Interfaces* 2 (2015) 1400529.
- S.R. Naqvi, G.S. Rao, W. Luo, R. Ahuja, T. Hussain, *ChemPhysChem* 18 (2017) 513–518.
- J. Zhu, H. Wang, J. Liu, L. Ouyang, M. Zhu, *Nanotechnology* 28 (2017) 115604.
- J. Zhu, H. Wang, W. Cai, J. Liu, L. Ouyang, M. Zhu, *Int. J. Hydrogen Energy* 42 (2017) 15790–15798.
- K. Zhang, Y. Feng, F. Wang, Z. Yang, J. Wang, *J. Mater. Chem. C* 5 (2017) 11992–12022.
- L. Wang, P. Hu, Y. Long, Z. Liu, X. He, J. Mater. Chem. A 5 (2017) 22855–22876.
- D. Liu, M.W. Zhang, W.J. Xie, L. Sun, Y. Chen, W.W. Lei, *Catal. Sci. Technol.* 6 (2016) 8309–8313.
- C. Lee, S. Bhandari, B. Tiwari, N. Yapici, D. Zhang, Y. Yap, *Molecules* 21 (2016) 922.
- Q. Weng, X. Wang, Y. Bando, D. Golberg, *Chem. Soc. Rev.* 45 (2016) 3989–4012.
- Z. He, C. Kim, L. Lin, T.H. Jeon, S. Lin, X. Wang, W. Choi, *Nano Energy* 42 (2017) 58–68.
- W. Lei, V.N. Mochalin, D. Liu, S. Qin, Y. Gogotsi, Y. Chen, *Nat. Commun.* 6 (2015) 8849.
- Y. Wu, Y. Xue, S. Qin, D. Liu, X. Wang, X. Hu, J. Li, X. Wang, Y. Bando, D. Golberg, Y. Chen, Y. Gogotsi, W. Lei, *ACS Appl. Mater. Interfaces* 9 (2017) 43163–43170.
- W. Lei, D. Portehault, D. Liu, S. Qin, Y. Chen, *Nat. Commun.* 4 (2013) 1777.
- W. Yingcheng, W. Peiwen, C. Yanhong, H. Jing, L. Hongping, L. Linjie, J. Wei, Z. Beibei, L. Huaming, Z. Wenshuai, *Nanotechnology* 29 (2018) 025604.
- D. Lee, B. Lee, K.H. Park, H.J. Ryu, S. Jeon, S.H. Hong, *Nano Lett.* 15 (2015)

1238–1244.

[63] W.-Q. Han, R. Brutchev, T.D. Tilley, A. Zettl, *Nano Lett.* 4 (2004) 173–176.

[64] Z. Tong, D. Yang, Z. Li, Y. Nan, F. Ding, Y. Shen, Z. Jiang, *ACS Nano* 11 (2017) 1103–1112.

[65] P. Dibandjo, L. Bois, F. Chassagneux, D. Cornu, J.M. Letoffe, B. Toury, F. Babonneau, P. Miele, *Adv. Mater.* 17 (2005) 571–574.

[66] A. Vinu, M. Terrones, D. Golberg, S. Hishita, K. Ariga, T. Mori, *Chem. Mater.* 17 (2005) 5887–5890.

[67] S. Schlienger, J. Alauzun, F. Michaux, L. Vidal, J. Parmentier, C. Gervais, F. Babonneau, S. Bernard, P. Miele, J.B. Parra, *Chem. Mater.* 24 (2012) 88–96.

[68] M. Maleki, A. Beitollahi, J. Javadpour, N. Yahya, *Ceram. Int.* 41 (2015) 3806–3813.

[69] J. Li, X. Xiao, X. Xu, J. Lin, Y. Huang, Y. Xue, P. Jin, J. Zou, C. Tang, *Sci. Rep.* 3 (2013) 3208.

[70] P. Wu, W. Zhu, Y. Chao, J. Zhang, P. Zhang, H. Zhu, C. Li, Z. Chen, H. Li, S. Dai, *Chem. Commun.* 52 (2016) 144–147.

[71] Q. Li, T. Yang, Q. Yang, F. Wang, K.-C. Chou, X. Hou, *Ceram. Int.* 42 (2016) 8754–8762.

[72] A. Nag, K. Raidongia, K.P.S.S. Hembram, R. Datta, U.V. Waghmare, C.N.R. Rao, *ACS Nano* 4 (2010) 1539–1544.

[73] S. Marchesini, A. Regoutz, D. Payne, C. Petit, *Microporous Mesoporous Mater.* 243 (2017) 154–163.

[74] S. Marchesini, C.M. McGilvery, J. Bailey, C. Petit, *ACS Nano* 11 (2017) 10003–10011.

[75] C. Tang, J. Li, Y. Bando, C. Zhi, D. Golberg, *Chem. Asian J.* 5 (2010) 1220–1224.

[76] Y. Ide, F. Liu, J. Zhang, N. Kawamoto, K. Komaguchi, Y. Bando, D. Golberg, *J. Mater. Chem. A* 2 (2014) 4150.

[77] D. Liu, M. Zhang, W. Xie, L. Sun, Y. Chen, W. Lei, *Appl. Catal. B: Environ.* 207 (2017) 72–78.

[78] M. Wang, M. Li, L. Xu, L. Wang, Z. Ju, G. Li, Y. Qian, *Catal. Sci. Technol.* 1 (2011) 1159.

[79] J. Choi, D.A. Reddy, T.K. Kim, *Ceram. Int.* 41 (2015) 13793–13803.

[80] W. Wu, X. Lv, J. Wang, J. Xie, *J. Colloid Interf. Sci.* 496 (2017) 434–445.

[81] H. Wang, X. Qiao, J. Chen, X. Wang, S. Ding, *Mater. Chem. Phys.* 94 (2005) 449–453.

[82] C. Zhu, J. Zheng, L. Fang, P. Hu, Y. Liu, X. Cao, M. Wu, *J. Mol. Catal. A-Chem.* 424 (2016) 135–144.

[83] J. Chen, J. Zhu, Z. Da, H. Xu, J. Yan, H. Ji, H. Shu, H. Li, *Appl. Surf. Sci.* 313 (2014) 1–9.

[84] X.-f. Wu, Z.-h. Zhao, Y. Sun, H. Li, C.-x. Zhang, Y.-j. Wang, Y. Liu, Y.-d. Wang, X.-y. Yang, X.-d. Gong, *J. Nanopar. Res.* 19 (2017).

[85] J. Wang, J. Shen, D. Fan, Z. Cui, X. Lü, J. Xie, M. Chen, *Mater. Lett.* 147 (2015) 8–11.

[86] X. Lv, J. Wang, Z. Yan, D. Jiang, J. Liu, *J. Mol. Catal. A-Chem.* 418 (2016) 146–153.

[87] L. Jiang, X. Yuan, G. Zeng, Z. Wu, J. Liang, X. Chen, L. Leng, H. Wang, H. Wang, *Appl. Catal. B: Environ.* 221 (2018) 715–725.

[88] Z. He, C. Kim, L. Lin, T.H. Jeon, S. Lin, X. Wang, W. Choi, *Nano Energy* 42 (2017) 58–68.

[89] X. Fu, Y. Hu, Y. Yang, W. Liu, S. Chen, J. Hazard, *Mater.* 244 (2013) 102–110.

[90] X. Fu, Y. Hu, T. Zhang, S. Chen, *Appl. Surf. Sci.* 280 (2013) 828–835.

[91] R. Zhang, J. Wang, P. Han, *J. Alloys Compd.* 637 (2015) 483–488.

[92] W. Xie, M. Zhang, D. Liu, W. Lei, L. Sun, X. Wang, *ACS Sustain. Chem. Eng.* 5 (2017) 1392–1399.

[93] Z. Chen, X. Chen, J. Di, Y. Liu, S. Yin, J. Xia, H. Li, *J. Colloid Interf. Sci.* 492 (2017) 51–60.

[94] J. Di, J. Xia, M. Ji, B. Wang, S. Yin, Q. Zhang, Z. Chen, H. Li, *Appl. Catal. B: Environ.* 183 (2016) 254–262.

[95] B. Wang, J. Di, J. Xia, L. Xu, H. Xu, Q. Zhang, Z. Chen, H. Li, *Mater. Technol.* 31 (2016) 463–470.

[96] D. Liu, Z. Jiang, C. Zhu, K. Qian, Z. Wu, J. Xie, *Dalton Trans.* 45 (2016) 2505–2516.

[97] S. Ding, D. Mao, S. Yang, F. Wang, L. Meng, M. Han, H. He, C. Sun, B. Xu, *Appl. Catal. B: Environ.* 210 (2017) 386–399.

[98] S. Meng, X. Ye, X. Ning, M. Xie, X. Fu, S. Chen, *Appl. Catal. B: Environ.* 182 (2016) 356–368.

[99] X. Li, F. Qi, Y. Xue, C. Yu, H. Jia, Y. Bai, S. Wang, Z. Liu, J. Zhang, C. Tang, *Rsc Adv.* 6 (2016) 99165–99171.

[100] J. Gu, J. Yan, Z. Chen, H. Ji, Y. Song, Y. Fan, H. Xu, H. Li, *Dalton Trans.* 46 (2017) 11250–11258.

[101] M. Sun, Q. Fu, L. Gao, Y. Zheng, Y. Li, M. Chen, X. Bao, *Nano Res.* 10 (2017) 1403–1412.

[102] L. Gao, Y. Wang, H. Li, Q. Li, N. Ta, L. Zhuang, Q. Fu, X. Bao, *Chem. Sci.* 8 (2017) 5728–5734.

[103] N. Sagara, S. Kamimura, T. Tsubota, T. Ohno, *Appl. Catal. B: Environ.* 192 (2016) 193–198.

[104] C. Huang, C. Chen, M. Zhang, L. Lin, X. Ye, S. Lin, M. Antonietti, X. Wang, *Nature Commun.* 6 (2015) 7698.

[105] S. Thaweesak, S. Wang, M. Lyu, M. Xiao, P. Peerakiatkajohn, L. Wang, *Dalton Trans.* 46 (2017) 10714–10720.

[106] M. Nasr, R. Viter, C. Eid, R. Habchi, P. Miele, M. Bechelany, *New J. Chem.* 41 (2017) 81–89.

[107] H. Xu, Z. Wu, M. Ding, X. Gao, *Mater. Des.* 114 (2017) 129–138.

[108] B. Singh, G. kaur, P. Singh, K. Singh, J. Sharma, M. Kumar, R. Bala, R. Meena, S.K. Sharma, A. Kumar, *New J. Chem.* 41 (2017) 11640–11646.

[109] H. Si, G. Lian, J. Wang, L. Li, Q. Wang, D. Cui, C.P. Wong, *ACS Appl. Mater. Interfaces* 8 (2016) 1578–1582.

[110] D. Liu, W. Cui, J. Lin, Y. Xue, Y. Huang, J. Li, J. Zhang, Z. Liu, C. Tang, *Catal. Commun.* 57 (2014) 9–13.

[111] X.-F. Wu, H. Li, Y. Sun, Y.-J. Wang, C.-X. Zhang, J.-Z. Su, J.-R. Zhang, F.-F. Yang, Y. Zhang, J.-C. Pan, *Appl. Phys. A* 123 (2017) 709.

[112] J. Yan, J. Gu, X. Wang, Y. Fan, Y. Zhao, J. Lian, Y. Xu, Y. Song, H. Xu, H. Li, *Rsc Adv.* 7 (2017) 25160–25170.

[113] F. Ma, G. Zhao, C. Li, T. Wang, Y. Wu, J. Lv, Y. Zhong, X. Hao, *CrystEngComm* 18 (2016) 631–637.

[114] C. Zhu, J. Zheng, L. Fang, P. Hu, Y. Liu, X. Cao, M. Wu, *J. Mol. Catal. A: Chem.* 424 (2016) 135–144.

[115] M. Ji, J. Xia, J. Di, Y. Liu, R. Chen, Z. Chen, S. Yin, H. Li, *Chem. Eng. J.* 331 (2018) 355–363.

[116] W. Li, Q. Wang, L. Huang, Y. Li, Y. Xu, Y. Song, Q. Zhang, H. Xu, H. Li, *Rsc Adv.* 5 (2015) 88832–88840.

[117] S. Ding, D. Mao, S. Yang, F. Wang, L. Meng, M. Han, H. He, C. Sun, B. Xu, *Appl. Catal. B: Environ.* 210 (2017) 386–399.

[118] H. Xu, Z. Wu, M. Ding, X. Gao, *Mater. Des.* 114 (2017) 129–138.

[119] W. Xie, M. Zhang, D. Liu, W. Lei, L. Sun, X. Wang, *J. Photochem. Photobiol., A* 333 (2017) 165–173.

[120] X. Wang, K. Maeda, A. Thomas, K. Takanabe, G. Xin, J.M. Carlsson, K. Domen, M. Antonietti, *Nat. Mater.* 8 (2009) 76–80.

[121] Y. Wang, X. Wang, M. Antonietti, *Angew. Chem. Int. Ed.* 51 (2012) 68–89.

[122] L. Jiang, X. Yuan, G. Zeng, J. Liang, X. Chen, H. Yu, H. Wang, Z. Wu, J. Zhang, T. Xiong, *Appl. Catal. B: Environ.* 227 (2018) 376–385.

[123] L. Jiang, X. Yuan, G. Zeng, Z. Wu, J. Liang, X. Chen, L. Leng, H. Wang, H. Wang, *Appl. Catal. B: Environ.* 221 (2018) 715–725.

[124] V. Štengl, J. Henych, M. Slušná, *J. Nanomater.* 2016 (2016) 1–12.